HHS Public Access

Author manuscript

Bone. Author manuscript; available in PMC 2017 September 01.

Published in final edited form as:

Bone. 2016 September ; 90: 69–79. doi:10.1016/j.bone.2016.05.014.

Low Intensity Vibration Mitigates Tumor Progression and Protect Bone Quantity and Quality in a Murine Model of Myeloma

Gabriel M. Pagnotti, PhD[1], **M. Ete Chan, PhD**[1], **Benjamin J. Adler, PhD**[1], **Kenneth R. Shroyer, MD, PhD**[2], **Janet Rubin, MD**[3], **Steven D. Bain, PhD**[4], and **Clinton T. Rubin, PhD**[1]

[1]Department of Biomedical Engineering; Stony Brook University; Stony Brook, NY, 11794-5281

[2]Department of Pathology; Stony Brook University; Stony Brook, NY, 11794-2580

[3]Department of Medicine; University of North Carolina; Chapel Hill, NC, 27599

[4]Department of Orthopedics & Sports Medicine; University of Washington; Seattle, WA, 98104-2499

Abstract

Myeloma facilitates destruction of bone and marrow. Since physical activity encourages musculoskeletal preservation we evaluated whether low-intensity vibrations (LIV), a component of mechanical signaling, could protect bone and marrow during myeloma progression. Immunocompromised-mice (n=25) were injected with human-myeloma cells, while 8 (AC) were saline-injected. Myeloma-injected mice (LIV; n=13) were subjected to daily-mechanical loading (15min/d; 0.3g @ 90Hz) while 12 (MM) were sham-handled. At 8w, femurs had 85% less trabecular bone volume (BV) fraction in MM versus AC, yet only a 21% decrease in LIV as compared to as compared to AC, reflecting a 76% increase versus MM. Cortical BV was 21% and 15% lower in MM and LIV, respectively, than AC; LIV showing 30% improvement over MM. Similar outcomes were observed in the axial skeleton, showing a 35% loss in MM with a 27% improved retention of bone in L5 of LIV-treated mice as compared to MM. Transcortical-perforations in the femur from myeloma-induced osteolysis were 9× higher in MM versus AC, reduced by 57% in LIV. Serum-TRACP5b, 61% greater in MM versus AC, rose by 33% in LIV compared to AC, a 45% reduction in activity when compared to MM. Histomorphometric analyses of trabecular bone demonstrated a 70% elevation in eroded surfaces of MM versus AC, while measures in LIV were 58% below those in MM. 72% of marrow in the femur of MM mice

Corresponding Author: Clinton T. Rubin, PhD, Department of Biomedical Engineering, Stony Brook University, Stony Brook, New York 11794-5281, Phone: (631)-632-2302, Fax: (631)-632-8577, clinton.rubin@stonybrook.edu.

Conflict of Interest:

C. T. Rubin is a founder of Marodyne Medical, Inc. and has a USPTO application under review for the ability of mechanical signals to control metabolic disorders. The other authors declare no competing interests.

Authors' Roles

Study Design: CTR and GMP. Study Conduct and Data Collection: GMP. Data Analysis: CTR, GMP, KRS, and SDB. Data Interpretation: CTR, GMP, JER, KRS, and SDB. Drafting Manuscript: CTR and GMP. Revising Manuscript Content: CTR, MEC, BJA, GMP, JER, KRS, and SDB. Approving Final Version of Manuscript: CTR, GMP, JER, and KRS. GMP takes responsibility for the integrity of the data analysis.

contained tumor, contrasted by a 31% lower burden in LIV. MM mice (42%) presented advanced-stage necrosis of marrow in the tibia while present in just 8% of LIV. Myeloma infiltration inversely correlated to measures of bone quality, while LIV slowed systemic myeloma-associated decline in bone quality and inhibited tumor progression through the hindlimbs.

1. Introduction

In the United States, there is a 0.7% lifetime risk of acquiring multiple myeloma, a cancer that forms from plasma cells and accumulates within the bone marrow, thus crowding out healthy blood cells (1, 2). Myeloma is the second most prevalent hematologic malignancy (3, 4), representing approximately 15% of all hematologic cancers (5), with 27 000 new U.S. cases projected to be diagnosed this year (1). Recently developed therapeutics have increased 5-year survival to 44%, yet over 11 000 patients still die of this disease each year in the U.S. Bone resorption is one of the defining comorbidities of myeloma, compromising skeletal quality and increasing fracture susceptibility in those with the disease (6, 7). Spread of malignant plasma cells through the bone marrow (BM) space also disrupts resident hematopoietic progenitors and weakens the immune response (8–10), and, in aggregate, consequences of BM crowding by myeloma contributes to decreased quality-of-life despite advances in treatment.

Pathologically, myeloma is characterized by a marked increase in plasma cell density within the BM (11–13), with tumor cell invasion disrupting the tightly orchestrated mechanisms that control bone remodeling while simultaneously creating an environment conducive to osteolytic lesions (4, 14). Further, the transformation of the BM into a tumor supportive niche leaves a less viable milieu for the mesenchymal stem cell population (MSC) that are critical for tissue regeneration, and hematopoietic stem cells (HSC) central to hematopoiesis and myelopoiesis (11, 15).

Cancer progression and the array of treatment strategies employed to manage the disease often result in a significant challenge to the skeleton (16–19). The long-term, catabolic impact of chemotherapy, irradiation, and immunosuppressive therapies on bone endpoints contribute heavily to osteopenia (20), especially for the very young (18, 21), frail elderly (22), and immunosuppressed (23). Routine treatment strategies, from high-dose chemotherapy to fractionated radiotherapies (24, 25), are aimed at slowing tumor expansion, but each approach is limited by adverse effects. For example, while irradiation is effective in combating tumor burden (24), it degrades the bone matrix (20) and damages the spectra of cellular constituents which govern bone remodeling (26). Chemotherapy diminishes tumor burden but, amongst other side effects, can be associated with renal toxicity and pancytopenia (25, 27). Extensive radiation and/or chemotherapy may necessitate BM transplantation, increasing likelihood of secondary side effects (i.e., graft-vs.-host disease, acute myelodysplastic leukemia, or myelodysplastic syndrome) (28, 29). Glucocorticoids (e.g. Dexamethasone) are efficacious in diminishing tumor burden, primarily as a function of dosing, yet, high-dose and/or chronic use are heavily associated with toxicity and result in osteoporotic bone (30, 31) by inducing apoptosis in osteoblasts and osteocytes (32). Immunosuppressive agents (e.g., corticosteroids) are administered as primary therapy or to

permit graft tolerance (e.g. BM transplantation) but, in doing so, predispose the patient to infection. Anti-resorptives (e.g., bisphosphonates) have been shown to mitigate bone loss but are limited by inconsistent outcomes and negative side effects of short and long-term use, including osteonecrosis of the jaw and atypical fractures (33, 34).

In contrast to pharmacological-centric therapies, exercise is recognized as a non-drug deterrent of cancer, as well as a means to protect musculoskeletal health. Indeed, the attributes of physical activity have helped promote it as a foundation of any therapeutic plan (35–37). Paradoxically, for cancer patients already at risk for developing a fracture, even a moderate exercise regimen may precipitate the fractures that the treatment is prescribed to prevent. In an effort to incorporate non-drug strategies for those with a compromised musculoskeletal system, low-intensity vibration (LIV), a mechanical signal which mimics the dynamics of muscle contraction, has been shown to protect bone quality in a murine model susceptible to ovarian cancer (38). LIV's effects have been observed in both *in vitro* and *in vivo* systems to promote highly-ordered tissue synthesis (39, 40), upregulate musculoskeletal quality (41–43), and enhance cytoskeletal architecture of precursor bone cells (44, 45), while preserving the viability of the BM niche (46–48). Previous work by our group and others have demonstrated LIV as having an anabolic effect that encourages, at the level of the MSC, lineage differentiation towards osteogenesis and away from an adipogenic phenotype (49, 50). Contrarily, in the absence of mechanical loading, administration of LIV has been shown to reduce osteoclast activity across the endosteal surface (51) On the order of the cell, LIV has been shown to both decrease resorptive activity while also enhancing cytoskeletal proteins (52). To determine whether LIV is an effective agent against bone loss associated with myeloma, a xenograft mouse model was developed and, with the disease allowed to progress for 8w, quantified to what degree osteolysis and tumor progression had been influenced.

2. Materials and Methods

2.1. Human Myeloma Cell Culture and Expansion

A cryogenically preserved human-myeloma cell line (U266β1; *ATCC*; Manassas, VA, USA), was thawed and cultured using aseptic techniques. Centrifugation was used to separate (4°C, 125g, 6min) cell pellets from media containing dimethyl-sulfoxide (DMSO). Pellets were resuspended in a 25cm^2 tissue culture flask with 10mL of growth media and incubated horizontally (37°C in 5% CO_2 atmosphere). Cell viability was quantified every 3d using an automated cytometer (Countess; *Invitrogen;* Rockville, MD, USA) until confluence (~97% viability), at which time the cell suspension was centrifuged (24°C, 2 200rpm, 5min), resuspended, and split 1:3 into 75cm^2 tissue culture flasks. According to manufacturer's recommendations, subcultures were maintained at a density of 3.5×10^5–1×10^6 cells/mL until day of injection.

2.2. Murine Model

All mice were individually housed. Power calculations were performed to account for effect-size (0.25) and for statistical power of at least 0.8. Age-Matched Control (AC; n=8), Myeloma-Injected (MM; n=12), and Myeloma-Injected treated with Low Intensity Vibration

(LIV; n=13) groups were distributed using a *Matlab* (*The MathWorks, Inc.*; Natick, MA, USA) algorithm that randomizes samples by weight matching. U266β1 cells were inoculated intravenously via tail vein into 7w-old, male immunodeficient NSG mice (NOD.Cg-*Prkdc*^{scid} *Il2rg*^{tm1Wjl}/SzJ; *The Jackson Laboratory;* Bar Harbor, ME, USA) (53). 25 NSG mice (MM and LIV) were injected with 0.3cc of 2×10^6 U266β1 via a sterile saline vehicle, while AC mice were injected with 0.3cc of sterile saline as control. Of the 25 U266β1-injected mice, 13 were subjected to 8w of LIV, while the remaining 12 received sham-LIV (MM). Criteria were established to exclude tissue samples from analyses if the associated mouse died prematurely, else all samples were utilized. Mice were maintained in accordance with the Institutional Animal Care and Use Committee guidelines at Stony Brook University and the NIH Guide for the Care and Use of Laboratory Animals.

2.3. Daily Mechanical Loading Protocol

Loading regimens commenced 4hrs post-inoculation providing a rest period in order to mitigate stress induced from handling. Mice assigned to the mechanical loading regimen were subject to LIV ($0.3g \pm 0.025$ @ 90Hz, where 1g = Earth's gravitational field or $9.8 m/s^2$) (38, 47, 51), for 15min/d, 5d/w, while AC and MM groups underwent identical handling and loading protocols as LIV mice but without activation of the platform. The daily loading regimen consisted of placing mice into individual 12cm×12cm containers on a fixed, vertically-oscillating platform (*Marodyne Medical*; Tampa, FL, USA) to administer the LIV signal. Displacements required to produce accelerations at 90Hz are well below 100μm and are barely perceptible to human touch. The lead investigator was not blinded to the experimental groups during the delivery of LIV.

2.4. Tissue Harvest and Preservation

At the end of the 8w protocol, each mouse was anesthetized using isoflurane inhalation and whole blood collected via cardiac puncture. Blood was then heparinized and aliquoted (100μl) for FACS analysis after erythrocyte lysis (1× Pharmalyse; *BD Biosciences*, San Jose, CA, USA). Euthanasia was achieved by cervical dislocation. Left femora were briefly preserved on ice, and BM was extracted and isolated using Dulbecco's modified Eagle's supplemented medium (DMEM; *GIBCO;* Grand Island, NY, USA) containing 2% FBS, 10mM HEPES Buffer, and 1% penicillin–streptomycin ($DMEM^+$). Tissues for histological processing, including right femora and tibia, were fixed in 10% neutral buffered formalin, replaced at 48h with 70% ethanol, and subsequently sectioned. Bone specimens were decalcified (DECAL; *Decal*; Suffern, NY, USA) and 5μm paraffin-embedded sagittal cross-sections were stained with hematoxylin and eosin (H&E). Prevalence of MM and evaluation of tumor burden were determined via histologic examination, performed by a histopathologist (KRS) who was blinded to the status of any mouse's experimental regimen.

2.5. Flow Cytometric Analyses of Femoral Bone Marrow

Flow cytometric analyses (FACSAria Cytometer; *BD Pharmingen*; San Diego, CA, USA) utilized specific markers to isolate and quantify cells of both the lymphoid and myeloid lineages. As reported, the FACS data represents the average of all cell populations quantified separately for each mouse across each group. Since the immune deficient mice do not have viable, native plasma cells, FACS analysis was performed using an antibody for the surface

marker CD138 (syndecan-1), a cell-membrane protein specific to all plasma cells, to determine engraftment efficacy of the myeloma cells that had been injected (54). Peripheral blood was tested for the presence of $CD138^+$ cells. Whole marrow from femora were individually isolated and homogenized in 3mL of $DMEM^+$ in order to maximize cell viability before tissue processing. Subsequent steps consisted of macroparticle filtration, erythrocyte lysis, and washing with 1mL of DPBS and centrifugation (4°C, 2000rpm, 10min). 2×10^6 marrow cells from each sample were quantified from each mouse using an automated cell counter (Scepter; *Millipore*; Billerica, MA, USA), fixed with 1% NBF in Hank's Buffered Salt Solution, and stained for specific hematopoietic surface markers. Human myeloma cells ($CD138^+$: Catalog #561703, *BD Pharmingen*), mature macrophages ($CD11c^+$/$F4\text{-}80^+$: #557401*, BD Pharmingen* & Catalog #45-4801-82; EBioscience.com; San Diego, CA, USA), and a marker for precursor natural killer (NK) cells ($NK1.1^+$: Catalog #553164, *BD Pharmingen*) were quantified based on fluorescent antibody-tagging.

2.6. Histological Evaluation of Tumor Burden

Histologic sections were used to estimate the tumor area fraction (percent of native marrow replaced with myeloma cells). Images were taken of longitudinal, paraffin-embedded H&E-stained sections of bone (20×) using digital histological software (Aperio ImageScope; *Leica Biosystems;* Buffalo Grove, IL). Marrow area (MA), tumor area (TA), and necrotic tumor area (NT) were individually demarcated using image-processing software (ImageJ; *National Institutes of Health*; Bethesda, MD, USA). MA was defined as the non-cancellous tissue bounded by the endosteal surface of the cortex, from the length of the diaphyseal midshaft to the distal end of the femur. TA was outlined within the MA and quantified. Additionally, regions of NT were outlined and quantified from within the TA. Immunohistochemistry on formalin-fixed paraffin embedded bone sections was performed to validate the presence of tumor using an antibody for surface-bound CD138 at a 1:25 dilution (PA5-32305; *Thermo Scientific*, Rockford, IL). Annexin V (ab14196; *Abcam Inc.*; Cambridge, MA) was used at a dilution of 1:500 as a marker for validation of necrotic tumor in the tibial bone marrow.

2.7. High-Resolution Micro-Computed Tomography and Analyses of Cortical and Trabecular Bone Morphology

Quantity and quality of bone across the distal femoral, proximal tibial metaphysis, and L5 vertebrae were measured *ex vivo* using X-ray micro-computed tomography (μCT40; *Scanco Medical*; Wayne, PA, USA). X-ray source voltage was set to 55kVp, current set to 145μA, integration time was 300ms, and voxel size was 10μm. Parameters measured were as follows: trabecular bone volume fraction (Tb.BV/TV), cortical bone volume fraction (Ct.BV/TV), and the number of transcortical perforations. Starting 700μm distal to the epiphyseal growth plate in the tibia and 700μm proximal to the growth plate of the femur, 1 000μm of metaphyseal bone was evaluated. A 500μm uniform core of trabecular bone, taking care not to include primary spongiosa, was evaluated within the vertebral body of the L5 vertebrae. Thresholds for each slice were set exclusively to separate cortical and trabecular bone using an automated script (55). Reconstructed solid 3D images were then used to quantify bone microarchitecture and the number of perforations that extended from the periosteum to the endosteal surface. Digitally slicing the 3D reconstructed image along

the sagittal and transverse axes revealed perforations, and these were included if they breached the periosteal surface.

2.8. Static Histomorphometry

2D-point counting stereology was used to quantify the bone resorbing and bone forming surfaces in trabecular bone of the distal femur. Briefly, a 36-point Merz Grid was superimposed on the region-of-interest at 200× magnification (BV/TV was quantified at 100× magnification) and grid intersections with either eroded surfaces per trabecular surface (ES/TS: presence of multinucleated osteoclasts and/or clear evidence of trabecular resorption pits) or forming surface per trabecular surface (OB/TS: cuboidal, basophilic cells on trabecular bone surfaces) were determined as a percentage of the total intersections with trabecular bone surface. Resorption surface was defined as trabecular surfaces undergoing resorption by multinucleated osteoclasts and/or crenated trabecular surfaces with clear evidence of osteoclast resorption (i.e. resorption lacunae/scalloped surfaces with no evidence of osteoblast formation). All readings were performed blind to the experimental history of the specimen. These analyses were performed by a histomorphometrist (SDB) who was blinded to the status of any mouse's experimental regimen.

2.9. Osteoclast Activity (Serum-TRACP5b)

To provide a systemic index of osteolysis, serum was isolated from peripheral blood through centrifugation (4°C, 2 500rpm, 10min), aliquoted, and stored at −80°C. Samples were thawed to room temperature before performing an immunoassay to quantify osteoclast (OC)-secreted tartrate-resistant acid phosphatase (TRACP5b) (MouseTRAP; *Immunodiagnostics*; Scottsdale, AZ, USA). The assay was performed according to manufacturer's instructions. Mean absorbance was fit to a standard curve to obtain the sample concentration.

2.10. Statistical Analyses

Group-wise comparisons were made between AC, MM, and LIV groups. All graphical data is presented as dot plots with bars representing means ± standard deviation. Significance ($\alpha<0.05$) between MM and LIV groups as a function of the presence and degree of pathology was determined using Student's two-tailed *t*-test. The Shapiro-Wilk test was used to confirm the normality of the FACS and micro-CT sample distribution. One-way ANOVA was performed for micro-CT, FACS, and TRACP5b analyses between AC, MM, and LIV, followed by Tukey's post-hoc test. Pearson's correlations were made using a 95% confidence interval ($p<0.05$). Variances in bone quantity and marrow between non-injected and injected animals were estimated to be significantly different as a function of pathology.

3. Results

3.1. Animal Habitus

None of the mice from any of the experimental groups were lost prematurely over the 8w experimental period. No significant differences were measured between groups in mouse weights or food consumption (Supplemental Fig. 1).

3.2. Expansion of Myeloma Across the Marrow Space was Suppressed by Mechanical Signals

The NSG mouse model is genetically prohibited from developing mature lymphocytes, including terminally-differentiated B cells (i.e. plasma cells) and mature NK cells; therefore, detection of viable plasma cells in the marrow is indicative of successful engraftment (53). As compared to AC marrow, which maintained a healthy, red phenotype, evaluation of the marrow from MM and LIV indicated regions ≥ 1mm where normal marrow had been displaced by confluent sheets of plasma cells (Fig. 1). Histologic evaluation in both MM and LIV mice showed that resulting displacement of resident marrow constituents was consistent with profound anemia, leukopenia, and neutropenia. Extending further into the host marrow, plasma cells became visibly diffuse amongst the reticulocyte, granulocyte, and erythrocyte populations.

Tumor burden infiltrated 72% ± 15% of the femoral marrow space in MM, as compared to a 50% ± 26% invasion in LIV (Fig. 1), indicating a 31% ($p<0.01$) suppression by the mechanical signals. 100% of MM (12/12) and LIV (13/13) mice contained myeloma in the tibia, with the tumor crowding into 63% and 62% of the marrow space for MM and LIV, respectively. Necrotic tumor, representing a later stage of the disease, was evident in 42% (n=5) MM mice tibiae, as compared to 8% (n=1) of LIV tibiae with evidence of necrosis (Fig. 2). Sites of necrosis across the bone marrow were observed in the mid-diaphysis and extending beyond the growth plate into the epiphysis using an antibody for Annexin V. Within the MM group, tumor necrosis accounted for 50% of the tumor quantified in the marrow. Necrotic tumor occupied 40% of the tibial marrow space of MM, as compared to only 8% in LIV. No necrosis was observed in the femur of either group.

Osteolysis was visible at sites adjacent to myeloma tumors and was evident across the endosteal surface of both MM and LIV, including deep cortical resorption pits that breached the cortex from the marrow space to the periosteal surface. Extensive resorption pits (Howship's lacunae) were evident along the endosteal surface of both MM and LIV, adjacent to the infiltrating tumor, which often coincided with the presence of disorganized, woven bone within the cortical shell.

3.3. LIV Reduced Myeloma Cell Populations within the Marrow Space but Did Not Disrupt Immune Cell Reactivity

FACS quantification of overall marrow cellularity yielded a uniform measurement across all groups (NSD between groups) (Fig. 3). Homing of the injected cells was observed in the marrow of all 25 of the U266β1-injected mice. As measured in the marrow from the left femur, $CD138^+$ cells were detected as 15× higher in MM as compared to AC, with LIV reducing this by 40% (9× increase as compared to AC). Precursor natural killer cells ($NK1.1^+$) were 13× ($p<0.003$) greater in both MM and LIV as compared to AC, whereas differences between MM and LIV were negligible. Total mature macrophages ($CD11c^+$/$F4\text{-}80^+$) were 61% ($p<0.05$) greater in MM as compared to AC, with LIV reducing this by 26% (a 45% increase compared to AC).

3.4. Bone Quality Disrupted by MM Disrupted by MM was Protected by LIV

Femora—Micro-CT analyses of the distal femur revealed the trabecular bone volume fraction (Tb.BV/TV) in MM was reduced by 86% ($p<0.001$) as compared to AC, whereas LIV was only 21% ($p<0.01$) lower than AC, reflecting a 76% ($p<0.01$) improvement as compared to MM (Fig. 4). Cortical bone volume fraction (Ct.BV/TV) of the distal femur of MM was 21% ($p<0.01$) lower than AC, as compared to a 15% (NSD) lower value in LIV compared to AC, reflecting a 30% ($p<0.01$) improvement of LIV compared to MM.

Tibiae—Micro-CT analyses of the proximal tibiae demonstrated a 70% ($p<0.001$) decrease in trabecular bone volume fraction (Tb.BV/TV) in MM versus AC. Tb.BV/TV in LIV mice was 62% (NSD) lower than AC, but the 27% higher amount was also not significantly different than MM. (Fig. 4).Tissue mineral density in the proximal tibia was 39% ($p<0.001$) lower in MM as compared to AC, but fell only 27% ($p<0.002$) in LIV.

Vertebrae—Tb.BV/TV in L5 vertebrae of MM mice were 35% ($p<0.001$) lower than in AC, while LIV mice had 17% (NSD) less bone than AC, a measure that was 27% ($p<0.05$) greater as compared to MM (Fig. 5). Trabecular connectivity density (Conn. Dens.) in MM was 36% ($p<0.05$) lower than in AC, whereas in LIV only 6% (NSD) reduction was measured in AC, or 47% ($p<0.05$) greater than those of MM. The number of trabeculae (Tb.N.) in the L5 of MM had decreased by 16% ($p<0.05$) versus AC while decreasing by just 5% (NSD) in LIV in comparison to AC, a mark that 13% (NSD) greater than MM. As a measure of bone quality, the structure model index (SMI) of MM mice was 37% ($p<0.01$) greater than in AC, and while the trabeculae of LIV was 31% ($p<0.05$) greater than in AC this measure was reduced by just 5% (NSD) in LIV versus MM.

Cortical Perforations of the Femur—Transcortical perforations in AC femora were 9.6× greater in MM as compared to AC, contrasted with a 4× increase in LIV (Fig. 6). This reflects a 57% ($p<0.002$) reduction of osteolytic perforations of the cortex in those mice subject to LIV. The number of transcortical perforations positively correlated to the percent area of tumor tissue in the femur ($R^2=0.284$; $p<0.0005$) (Fig. 6).

3.5. Elevated Osteoclast Activity with Myeloma was Suppressed by LIV

Based on histomorphometric analyses at the distal femur, no primary spongiosa were observed in MM, yet they were partially protected by LIV. (Fig. 7) Growth plates appeared disrupted in MM, and in several cases islands of mineralized cartilage were evident in bone marrow. The Tb.BV/TV measured in MM was 75% ($p<0.001$) lower than in AC, while LIV was 36% ($p<0.05$) below AC, resulting in 60% ($p<0.01$) greater BV/TV than in MM, reinforcing the results derived from CT (above). Eroded surface per trabecular surface (ES/TS) of MM was 70% ($p<0.05$) greater than AC, while LIV was 29% (NSD) below AC, and thus 58% ($p<0.0001$) below MM. Osteoblast number per trabecular surface (OBl/TS) was 14% (NSD) lower in MM as compared to AC, whereas LIV was 7% (NSD) greater than AC and 24% (NSD) greater than MM.

A systemic measure of osteoclast activity, serum-TRACP5b, rose by 61% ($p<0.001$) in MM as compared to AC. However, these levels had increased by only 33% ($p<0.05$) in LIV as compared to AC, yielding a 45% ($p=0.06$) reduction from that measured in MM (Fig. 8).

4. Discussion

4.1

The destruction of bone marrow by myeloma plasma cells facilitates cortical and trabecular resorption and transcortical perforations (11, 56), concurrently elevating fracture risk and perturbing the immune system. And while exercise is recognized as an effective non-drug means of suppressing both cancer and osteoporosis, strenuous activity for this patient population may induce the very fracture it is prescribed to prevent. Serving as a surrogate for exercise, this study was designed to evaluate if low intensity vibrations, a physical signal demonstrated to stimulate osteoblastogenesis and reduce adipogenesis (43, 47), as well as suppress osteoclast activity (57), could slow the precipitous drop in bone quality accompanying myeloma infiltration of bone without serving as an anabolic signal to the tumor. The data suggest these extremely low magnitude mechanical signals helped to protect the bone phenotype, with some evidence that the progression of the tumor itself was suppressed.

Tumor burden was significantly lower in the femur of LIV mice than in engrafted mice that did not receive the mechanical intervention. In an effort to differentiate the degree of cancer progression between groups, the histological grade of the BM tumor was noted as either viable or necrotic tumor, the latter accounting for 42% (n=5 of 12) of the observations in MM tibiae but just 8% of the engrafted animals treated with LIV (n=1 of 13). This late-stage pathology is consistent with a more advanced grade of symptomatic myeloma and reflected by the fact that regions of viable tumor were predominantly void of the cellular composition of healthy marrow (58, 59), where necrotic tumor occupied 40% of the tibial marrow space of MM, as compared to only 8% in LIV. No necrosis was observed in the femur of either group. Given that the marrow volume of the femur is approximately twice that of the tibia, this suggests that an early stage in the pathogenesis of the disease may be to crowd out the healthy marrow, and once that occurs, marrow necrosis begins as aggravated by the absence of a viable marrow to support it. Alternatively, it is entirely possible that spatially distinct marrow populations may account for the differential progression of the tumor in the tibia vs. the femur, as well as the distinct responses of these bones to the mechanical intervention (60). Extrapolating to the clinic, it suggests that any intervention that slows the crowding of the marrow by the tumor would, naturally, slow the inevitable advance of necrosis that follows.

Utilizing mechanical signals to mitigate skeletal decline as a comorbidity of cancer – and its treatments – while maintaining quality of life shows some potential as a future clinical strategy, perhaps in tandem with other interventions. The reduced tumor burden measured in the marrow of the femur of LIV mice suggests that preservation of the marrow microenvironment in turn may help protect the bone organ. This conclusion is supported by the correlation between tumor area and quality of bone (Fig. 6). Further, the marked reduction in transcortical perforations and resorptive surface measured in LIV mice (Fig. 7),

reinforces that myeloma is permissive to osteolysis but that mechanical signals can slow this pernicious decline in bone structure.

Through signaling pathways are not yet understood, it is possible that mechanical signals not only slow the disruption of the marrow space, but preserve key aspects of the balance of bone remodeling. While the disease state clearly elevates resorptive activity, the apparent absence of any rise in formative activity fails to keep pace with the loss of bone, suggesting a consequence of the disease is the ‘uncoupling’ of bone remodeling. The ability of LIV to suppress the elevation of osteoclast activity is supported by the demonstrated ability of these mechanical signals to decrease osteoclast recruitment in hindlimb unloaded animals (51), as well as preserve bone formation activity under systemic suppression of activity disabling conditions such as cerebral palsy (46, 48). It is also possible that through the mechanical biasing of mesenchymal and hematopoietic stem cell fate towards specific endpoints (e.g., osteoblastogenesis and lymphopoeisis, respectively), that these physical signals slow the engraftment of myeloma cells and the conscription of osteoclasts, both of which are critical to advancement of the disease and the skeletal complications that follow (61).

Serum TRACP5b and static histomorphometry data reinforce a pronounced catabolic consequence of myeloma on the skeleton, and support the anti-resorptive endpoints on bone morphology as measured with CT. Therefore, it is reasonable to suggest that LIV may provide a means of introducing protective mechanical signals to normalize the bone cellular process in the face of disease-specific perturbations of the balance of remodeling. That LIV failed to protect bone quality in the tibia of myeloma mice as well as that measured in the femur can be interpreted several ways. One possibility is that the volume of marrow in the tibial compartment is approximately half that of the femur, and that mechanical signals simply could not outpace the progression of the disease. That said, it is interesting that the level of actual necrosis in the tibia of myeloma mice that served as sham control was higher than that measured in LIV, suggesting at least some capacity to deter the late stages of the pathology was evident. Alternatively, or in conjunction, there is evidence of spatial differences of marrow, not only within a given bone (62), but between bones (60), as well as the capacity of mechanical signals to influence bone morphology at these different sites. With evidence of the consequences of the disease evident in the axial skeleton, with some salutary benefit of LIV to protect skeletal components remote from the site of vibration, suggests circulatory factors may also be at play.

This study has several limitations. Methods of ensuring adequate engraftment may have introduced a disproportionate burden of malignant cells to the marrow than that which occurs during natural progression of myeloma development (63–65). Immunodeficient models introduce key mutational defects in immune surveillance (66, 67) and offer compromised hematopoiesis, increasing consistency in human cell line engraftments (68). Specifically, severe combined immune deficient (SCID) mice are engineered with impaired T and B lymphocyte development and function (66, 69, 70). In this vein, it is important to highlight that, while cells of the innate immune system (i.e. macrophages, granulocytes) were genetically intact to combat the tumor burden, elements of adaptive immunity were not present to enhance natural defenses against the cancer progression (71–74), as was reflected

by the significant increases in precursor-NK cell ($NK1.1^+$) and mature macrophage ($CD11c^+/F4\text{-}80^+$) activity quantified by FACS in both MM and LIV (Fig. 3).

That only the hindlimbs and axial skeleton were evaluated precludes an estimate of overall impact on the skeleton and other organs, such as the spleen, which is a site associated with B cell maturity and plasma cell infiltration. With marked increase in TRACP5b measured in the myeloma mice invariably points to a systemic elevation of osteoclast activity as compared to AC counterparts, these levels were significantly reduced by the introduction of LIV. This view is supported, at least in part, by the marked reduction in bone quality in the femur and spine, and the capacity of LIV to protect these regions, as well as the histomorphometric evidence of reduced osteoclast activity in the mechanically stimulated mice.

Recent efforts have been made to develop immunocompetent models of myeloma, thereby retaining the animals' immunity (75). Nevertheless, many characteristics of this model, specifically compromised bone quality, damaged cortex, and marrow destruction, mirror the phenotypic outcomes of the native disease. Additionally, the advanced state of tumor burden when considered in light of a relatively short study duration was quite severe. These findings are byproducts of U266β1 alone and may vary across other myeloma cell lines, specifically those of a primary myeloma plasma cell.

And, of course, only one mechanical regimen was considered. It is entirely possible that other mechanical regimens, including exercise, could slow the progress of the disease, or that the introduction of refractory periods between LIV and/or exercise administration would augment the potential of mechanical signals to slow the pathology (76). It is encouraging, however, that mechanical signals, extremely low in intensity and brief in duration, could represent a salutary influence on skeletal quality, and may someday help curb the consequences of the disease in the human.

Perhaps the greatest limitation of the study is the extrapolation to the human condition. It was encouraging that a non-drug approach effectively slowed destruction of the bone phenotype without exacerbating the disease itself – and perhaps even serving to decelerate the rapid progression observed in this model. It cannot be emphasized strongly enough that this is a mouse model of a grave human disease, and over-interpretation of these data in that regard must be avoided. Nevertheless, a recent study which explores the use of LIV on children cancer survivors demonstrates that this mechanical intervention can be safely applied to the human to build bone density without compromising health (77). As combination therapies point towards improved outcomes, perhaps an effective clinical strategy may incorporate mechanical signals in the form of exercise or other physical modalities alongside chemotherapy or irradiation, to mitigate myeloma-associated osteolysis while combating tumor progression.

Morphological, histological and biochemical endpoints emphasize the destructive capacity of myeloma cells as they propagate, with profound consequences on bone quality and marrow viability. This murine model bearing myeloma resulted in aggressive osteolysis and rapid destruction of healthy marrow. Low intensity vibration, serving as a surrogate for

exercise, slowed the degradation of the bone and marrow phenotype and suppressed the invasion of the tumor.

Supplementary Material

Refer to Web version on PubMed Central for supplementary material.

Acknowledgments

Funding:

This work was supported by the U.S. National Institutes of Health through National Institute of Arthritis and Musculoskeletal and Skin Diseases Grants AR43498 and EB14351 and The Center for Biotechnology at Stony Brook University. We would like to acknowledge the technical support provided by the Research Histology Core Laboratory, Department of Pathology, and Stony Brook Medicine. Additionally, the authors would like to express their appreciation to the following people for their contributions: Mallory Korman, Christina Preece, Stephanie Burke, and Daniel Mockler of Stony Brook Pathology for histological and digital processing of tissue samples; Laurie Levine, Nick Ortiz, and Jean Rooney for oversight with animal care; and Kimberly DeCarr, Danielle E. Green, Danielle Frechette, Divya Krishnamoorthy, Tee Pamon, Vihitaben Patel, Jeyant and Alyssa Tuthill of Stony Brook's Biomedical Engineering Department for assistance during animal sacrifice and tissue processing.

References

1. American Cancer Society. Cancer Facts and Figures 2015. Atlanta: The Society; 2015.
2. Howlader, N.; N, A.; Krapcho, M.; Garshell, J.; Miller, D.; Altekruse, SF.; Kosary, CL.; Yu, M.; Ruhl, J.; Tatalovich, Z.; Mariotto, A.; Lewis, DR.; Chen, HS.; Feuer, EJ.; Cronin, KA., editors. SEER Cancer Statistics Review, 1975–2011. Bethesda, MD: National Cancer Institute; 2014. [Available from: http://seer.cancer.gov/csr/1975_2011/
3. Weinberg, RA. The biology of cancer. New York: Garland Science; 2007.
4. Giuliani N, Rizzoli V, Roodman GD. Multiple myeloma bone disease: Pathophysiology of osteoblast inhibition. Blood. 2006; 108(13):3992–6. [PubMed: 16917004]
5. Moreau P, San Miguel J, Ludwig H, Schouten H, Mohty M, Dimopoulos M, et al. Multiple myeloma: ESMO Clinical Practice Guidelines for diagnosis, treatment and follow-up. Ann Oncol. 2013; 24(Suppl 6):vi, 133–7.
6. Melton LJ 3rd, Kyle RA, Achenbach SJ, Oberg AL, Rajkumar SV. Fracture risk with multiple myeloma: a population-based study. J Bone Miner Res. 2005; 20(3):487–93. [PubMed: 15746994]
7. Saad F, Lipton A, Cook R, Chen YM, Smith M, Coleman R. Pathologic fractures correlate with reduced survival in patients with malignant bone disease. Cancer. 2007; 110(8):1860–7. [PubMed: 17763372]
8. Purton LE, Scadden DT. Osteoclasts eat stem cells out of house and home. Nat Med. 2006; 12(6): 610–1. [PubMed: 16761001]
9. Romano A, Conticello C, Cavalli M, Vetro C, La Fauci A, Parrinello NL, et al. Immunological dysregulation in multiple myeloma microenvironment. BioMed research international. 2014; 2014:198539. [PubMed: 25013764]
10. Ramos J, Lorsbach R. Hemophagocytosis by neoplastic plasma cells in multiple myeloma. Blood. 2014; 123(11):1634. [PubMed: 24761451]
11. Manier S, Sacco A, Leleu X, Ghobrial IM, Roccaro AM. Bone marrow microenvironment in multiple myeloma progression. Journal of biomedicine & biotechnology. 2012; 2012:157496. [PubMed: 23093834]
12. Roodman GD. Pathogenesis of myeloma bone disease. J Cell Biochem. 2010; 109(2):283–91. [PubMed: 20014067]
13. Fowler JA, Mundy GR, Lwin ST, Edwards CM. Bone marrow stromal cells create a permissive microenvironment for myeloma development: a new stromal role for Wnt inhibitor Dkk1. Cancer Res. 2012; 72(9):2183–9. [PubMed: 22374979]

14. Galson DL, Silbermann R, Roodman GD. Mechanisms of multiple myeloma bone disease. BoneKEy reports. 2012; 1:135. [PubMed: 23951515]
15. Nair JR, Rozanski CH, Lee KP. Under one roof: The bone marrow survival niche for multiple myeloma and normal plasma cells. Oncoimmunology. 2012; 1(3):388–9. [PubMed: 22737625]
16. Ramaswamy B, Shapiro CL. Osteopenia and osteoporosis in women with breast cancer. Semin Oncol. 2003; 30(6):763–75. [PubMed: 14663777]
17. Holmes SJ, Whitehouse RW, Clark ST, Crowther DC, Adams JE, Shalet SM. Reduced bone mineral density in men following chemotherapy for Hodgkin's disease. Br J Cancer. 1994; 70(2): 371–5. [PubMed: 8054287]
18. Sala A, Barr RD. Osteopenia and cancer in children and adolescents: the fragility of success. Cancer. 2007; 109(7):1420–31. [PubMed: 17326055]
19. Pfeilschifter J, Diel IJ. Osteoporosis due to cancer treatment: pathogenesis and management. J Clin Oncol. 2000; 18(7):1570–93. [PubMed: 10735906]
20. Green DE, Adler BJ, Chan ME, Lennon JJ, Acerbo AS, Miller LM, et al. Altered Composition of Bone as Triggered by Irradiation Facilitates the Rapid Erosion of the Matrix by Both Cellular and Physicochemical Processes. Plos One. 2013; 8(5)
21. Hogler W, Wehl G, van Staa T, Meister B, Klein-Franke A, Kropshofer G. Incidence of skeletal complications during treatment of childhood acute lymphoblastic leukemia: comparison of fracture risk with the General Practice Research Database. Pediatr Blood Cancer. 2007; 48(1):21–7. [PubMed: 16317756]
22. Baxter NN, Habermann EB, Tepper JE, Durham SB, Virnig BA. Risk of pelvic fractures in older women following pelvic irradiation. JAMA. 2005; 294(20):2587–93. [PubMed: 16304072]
23. Kubica AW, Brewer JD. Melanoma in immunosuppressed patients. Mayo Clin Proc. 2012; 87(10): 991–1003. [PubMed: 23036673]
24. Lu, JJ.; Brady, LW.; Abitbol, AA. Radiation oncology: an evidence-based approach. Berlin: Springer; 2008. p. xx, 675
25. Chabner, B.; Longo, DL. Cancer chemotherapy and biotherapy: principles and practice. 4th. Philadelphia: Lippincott Williams & Wilkins; 2006. p. xv, 879
26. Green DE, Adler BJ, Chan ME, Rubin CT. Devastation of adult stem cell pools by irradiation precedes collapse of trabecular bone quality and quantity. J Bone Miner Res. 2012; 27(4):749–59. [PubMed: 22190044]
27. Khan R, Apewokin S, Grazziutti M, Yaccoby S, Epstein J, van Rhee F, et al. Renal insufficiency retains adverse prognostic implications despite renal function improvement following Total Therapy for newly diagnosed multiple myeloma. Leukemia. 2015
28. Bishop MR. Hematopoietic stem cell transplantation. Introduction. Cancer treatment and research. 2009; 144:ix–x. [PubMed: 20695131]
29. Einhorn N. Acute leukemia after chemotherapy (melphalan). Cancer. 1978; 41(2):444–7. [PubMed: 272946]
30. Weinstein RS. Glucocorticoid-induced osteoporosis and osteonecrosis. Endocrinology and metabolism clinics of North America. 2012; 41(3):595–611. [PubMed: 22877431]
31. Weinstein RS. Clinical practice. Glucocorticoid-induced bone disease. The New England journal of medicine. 2011; 365(1):62–70. [PubMed: 21732837]
32. Weinstein RS, Nicholas RW, Manolagas SC. Apoptosis of osteocytes in glucocorticoid-induced osteonecrosis of the hip. The Journal of clinical endocrinology and metabolism. 2000; 85(8):2907–12. [PubMed: 10946902]
33. Cipriani C, Irani D, Bilezikian JP. Safety of osteoanabolic therapy: a decade of experience. J Bone Miner Res. 2012; 27(12):2419–28. [PubMed: 23165426]
34. Subbiah V, Madsen VS, Raymond AK, Benjamin RS, Ludwig JA. Of mice and men: divergent risks of teriparatide-induced osteosarcoma. Osteoporos Int. 2010; 21(6):1041–5. [PubMed: 19597911]
35. Wiggins MS, Simonavice EM. Cancer prevention, aerobic capacity, and physical functioning in survivors related to physical activity: a recent review. Cancer Manag Res. 2010; 2:157–64. [PubMed: 21188106]

36. Battaglini CL, Mills RC, Phillips BL, Lee JT, Story CE, Nascimento MG, et al. Twenty-five years of research on the effects of exercise training in breast cancer survivors: A systematic review of the literature. World journal of clinical oncology. 2014; 5(2):177–90. [PubMed: 24829866]
37. Alves CR, da Cunha TF, da Paixao NA, Brum PC. Aerobic exercise training as therapy for cardiac and cancer cachexia. Life Sci. 2014
38. Pagnotti GM, Adler BJ, Green DE, Chan ME, Frechette DM, Shroyer KR, et al. Low magnitude mechanical signals mitigate osteopenia without compromising longevity in an aged murine model of spontaneous granulosa cell ovarian cancer. Bone. 2012; 51(3):570–7. [PubMed: 22584009]
39. Gilsanz V, Wren TA, Sanchez M, Dorey F, Judex S, Rubin C. Low-level, high-frequency mechanical signals enhance musculoskeletal development of young women with low BMD. Journal of bone and mineral research: the official journal of the American Society for Bone and Mineral Research. 2006; 21(9):1464–74.
40. Rubin C, Turner AS, Mallinckrodt C, Jerome C, McLeod K, Bain S. Mechanical strain, induced noninvasively in the high-frequency domain, is anabolic to cancellous bone, but not cortical bone. Bone. 2002; 30(3):445–52. [PubMed: 11882457]
41. Sen B, Styner M, Xie Z, Case N, Rubin CT, Rubin J. Mechanical loading regulates NFATc1 and beta-catenin signaling through a GSK3beta control node. The Journal of biological chemistry. 2009; 284(50):34607–17. [PubMed: 19840939]
42. Thompson WR, Guilluy C, Xie Z, Sen B, Brobst KE, Yen SS, et al. Mechanically Activated Fyn Utilizes mTORC2 to Regulate RhoA and Adipogenesis in Mesenchymal Stem Cells. Stem Cells. 2013
43. Rubin C, Turner AS, Bain S, Mallinckrodt C, McLeod K. Anabolism. Low mechanical signals strengthen long bones. Nature. 2001; 412(6847):603–4. [PubMed: 11493908]
44. Uzer G, Pongkitwitoon S, Ete Chan M, Judex S. Vibration induced osteogenic commitment of mesenchymal stem cells is enhanced by cytoskeletal remodeling but not fluid shear. Journal of biomechanics. 2013; 46(13):2296–302. [PubMed: 23870506]
45. Sen B, Xie Z, Case N, Thompson WR, Uzer G, Styner M, et al. mTORC2 regulates mechanically induced cytoskeletal reorganization and lineage selection in marrow-derived mesenchymal stem cells. Journal of bone and mineral research: the official journal of the American Society for Bone and Mineral Research. 2014; 29(1):78–89.
46. Ward K, Alsop C, Caulton J, Rubin C, Adams J, Mughal Z. Low magnitude mechanical loading is osteogenic in children with disabling conditions. Journal of Bone and Mineral Research. 2004; 19(3):360–9. [PubMed: 15040823]
47. Luu YK, Capilla E, Rosen CJ, Gilsanz V, Pessin JE, Judex S, et al. Mechanical Stimulation of Mesenchymal Stem Cell Proliferation and Differentiation Promotes Osteogenesis While Preventing Dietary-Induced Obesity. Journal of Bone and Mineral Research. 2009; 24(1):50–61. [PubMed: 18715135]
48. Ozcivici E, Luu YK, Adler B, Qin YX, Rubin J, Judex S, et al. Mechanical signals as anabolic agents in bone. Nat Rev Rheumatol. 2010; 6(1):50–9. [PubMed: 20046206]
49. Luu YK, Pessin JE, Judex S, Rubin J, Rubin CT. Mechanical Signals As a Non-Invasive Means to Influence Mesenchymal Stem Cell Fate, Promoting Bone and Suppressing the Fat Phenotype. BoneKEy osteovision. 2009; 6(4):132–49. [PubMed: 22241295]
50. Luu YK, Capilla E, Rosen CJ, Gilsanz V, Pessin JE, Judex S, et al. Mechanical stimulation of mesenchymal stem cell proliferation and differentiation promotes osteogenesis while preventing dietary-induced obesity. Journal of bone and mineral research: the official journal of the American Society for Bone and Mineral Research. 2009; 24(1):50–61.
51. Ozcivici E, Luu YK, Rubin CT, Judex S. Low-level vibrations retain bone marrow's osteogenic potential and augment recovery of trabecular bone during reambulation. PloS one. 2010; 5(6):e11178. [PubMed: 20567514]
52. Rubin J, Fan X, Biskobing DM, Taylor WR, Rubin CT. Osteoclastogenesis is repressed by mechanical strain in an in vitro model. Journal of orthopaedic research: official publication of the Orthopaedic Research Society. 1999; 17(5):639–45. [PubMed: 10569471]

53. King M, Pearson T, Shultz LD, Leif J, Bottino R, Trucco M, et al. A new Hu-PBL model for the study of human islet alloreactivity based on NOD-scid mice bearing a targeted mutation in the IL-2 receptor gamma chain gene. Clin Immunol. 2008; 126(3):303–14. [PubMed: 18096436]
54. Chilosi M, Adami F, Lestani M, Montagna L, Cimarosto L, Semenzato G, et al. CD138/syndecan-1: a useful immunohistochemical marker of normal and neoplastic plasma cells on routine trephine bone marrow biopsies. Mod Pathol. 1999; 12(12):1101–6. [PubMed: 10619261]
55. Lublinsky S, Ozcivici E, Judex S. An automated algorithm to detect the trabecular-cortical bone interface in micro-computed tomographic images. Calcified tissue international. 2007; 81(4):285–93. [PubMed: 17828460]
56. Lemaire M, Deleu S, De Bruyne E, Van Valckenborgh E, Menu E, Vanderkerken K. The microenvironment and molecular biology of the multiple myeloma tumor. Advances in cancer research. 2011; 110:19–42. [PubMed: 21704227]
57. Xie L, Jacobson JM, Choi ES, Busa B, Donahue LR, Miller LM, et al. Low-level mechanical vibrations can influence bone resorption and bone formation in the growing skeleton. Bone. 2006; 39(5):1059–66. [PubMed: 16824816]
58. Kumar, V.; Abbas, AK.; Aster, JC.; Robbins, SL. Robbins basic pathology. 9th. Philadelphia, PA: Elsevier/Saunders; 2013. p. xii, 910
59. Zhu AX, Niesvizky R, Hedrick E, Fata F, Filippa DA, Michaeli J. Extensive bone marrow necrosis associated with multiple myeloma. Leukemia. 1999; 13(12):2118–20. [PubMed: 10602440]
60. Wallace IJ, Pagnotti GM, Rubin-Sigler J, Naeher M, Copes LE, Judex S, et al. Focal enhancement of the skeleton to exercise correlates with responsivity of bone marrow mesenchymal stem cells rather than peak external forces. The Journal of experimental biology. 2015; 218(Pt 19):3002–9. [PubMed: 26232415]
61. Yaccoby S, Wezeman MJ, Henderson A, Cottler-Fox M, Yi Q, Barlogie B, et al. Cancer and the microenvironment: myeloma-osteoclast interactions as a model. Cancer Res. 2004; 64(6):2016–23. [PubMed: 15026338]
62. Styner M, Pagnotti GM, Galior K, Wu X, Thompson WR, Uzer G, et al. Exercise Regulation of Marrow Fat in the Setting of PPARgamma Agonist Treatment in Female C57BL/6 Mice. Endocrinology. 2015; 156(8):2753–61. [PubMed: 26052898]
63. Sullivan PW, Salmon SE. Kinetics of tumor growth and regression in IgG multiple myeloma. J Clin Invest. 1972; 51(7):1697–708. [PubMed: 5040867]
64. Hokanson JA, Brown BW, Thompson JR, Drewinko B, Alexanian R. Tumor growth patterns in multiple myeloma. Cancer. 1977; 39(3):1077–84. [PubMed: 912647]
65. Salmon SE, Smith BA. Immunoglobulin synthesis and total body tumor cell number in IgG multiple myeloma. J Clin Invest. 1970; 49(6):1114–21. [PubMed: 4987170]
66. Mirandola L, Yu Y, Jenkins MR, Chiaramonte R, Cobos E, John CM, et al. Tracking human multiple myeloma xenografts in NOD-Rag-1/IL-2 receptor gamma chain-null mice with the novel biomarker AKAP-4. BMC Cancer. 2011; 11:394. [PubMed: 21923911]
67. Radl J, Croese JW, Zurcher C, Van den Enden-Vieveen MH, de Leeuw AM. Animal model of human disease. Multiple myeloma. Am J Pathol. 1988; 132(3):593–7. [PubMed: 3414786]
68. Swami A, Reagan MR, Basto P, Mishima Y, Kamaly N, Glavey S, et al. Engineered nanomedicine for myeloma and bone microenvironment targeting. Proc Natl Acad Sci U S A. 2014; 111(28):10287–92. [PubMed: 24982170]
69. Shultz LD, Lyons BL, Burzenski LM, Gott B, Chen X, Chaleff S, et al. Human lymphoid and myeloid cell development in NOD/LtSz-scid IL2R gamma null mice engrafted with mobilized human hemopoietic stem cells. J Immunol. 2005; 174(10):6477–89. [PubMed: 15879151]
70. Huang YW, Richardson JA, Tong AW, Zhang BQ, Stone MJ, Vitetta ES. Disseminated growth of a human multiple myeloma cell line in mice with severe combined immunodeficiency disease. Cancer Res. 1993; 53(6):1392–6. [PubMed: 8443818]
71. Van Camp B, Durie BG, Spier C, De Waele M, Van Riet I, Vela E, et al. Plasma cells in multiple myeloma express a natural killer cell-associated antigen: CD56 (NKH-1; Leu-19). Blood. 1990; 76(2):377–82. [PubMed: 1695113]

72. Pross HF, Baines MG. Spontaneous human lymphocyte-mediated cytotoxicity againts tumour target cells. I. The effect of malignant disease. International journal of cancer Journal international du cancer. 1976; 18(5):593–604. [PubMed: 825477]

73. Uchida A, Yagita M, Sugiyama H, Hoshino T, Moore M. Strong natural killer (NK) cell activity in bone marrow of myeloma patients: accelerated maturation of bone marrow NK cells and their interaction with other bone marrow cells. International journal of cancer Journal international du cancer. 1984; 34(3):375–81. [PubMed: 6592156]

74. Kennard J, Zolla-Pazner S. Origin and function of suppressor macrophages in myeloma. J Immunol. 1980; 124(1):268–73. [PubMed: 6965292]

75. Glavey SV, Manier S, Natoni A, Sacco A, Moschetta M, Reagan MR, et al. The sialyltransferase ST3GAL6 influences homing and survival in multiple myeloma. Blood. 2014; 124(11):1765–76. [PubMed: 25061176]

76. Sen B, Xie Z, Case N, Styner M, Rubin CT, Rubin J. Mechanical signal influence on mesenchymal stem cell fate is enhanced by incorporation of refractory periods into the loading regimen. Journal of biomechanics. 2011; 44(4):593–9. [PubMed: 21130997]

77. Mogil RJ, Kaste SC, Ferry RJ Jr, Hudson MM, Mulrooney DA, Howell CR, et al. Effect of Low-Magnitude, High-Frequency Mechanical Stimulation on BMD Among Young Childhood Cancer Survivors: A Randomized Clinical Trial. JAMA oncology. 2016; doi: 10.1001/jamaoncol.2015.6557

Highlights

- Bone and marrow quality were compromised in a murine model of multiple myeloma (MM).
- Reduced bone quality and increased cortical perforations correlated to increased tumor burden.
- Low intensity vibration (LIV) suppressed appendicular and axial skeletal damage provoked by MM.
- LIV mitigated tumor burden, including a reduction in marrow necrosis.
- TRACP5b and histologic evidence of resorptive surface were lower in LIV, indicating suppression of osteoclastic activity in MM subject to mechanical signals.

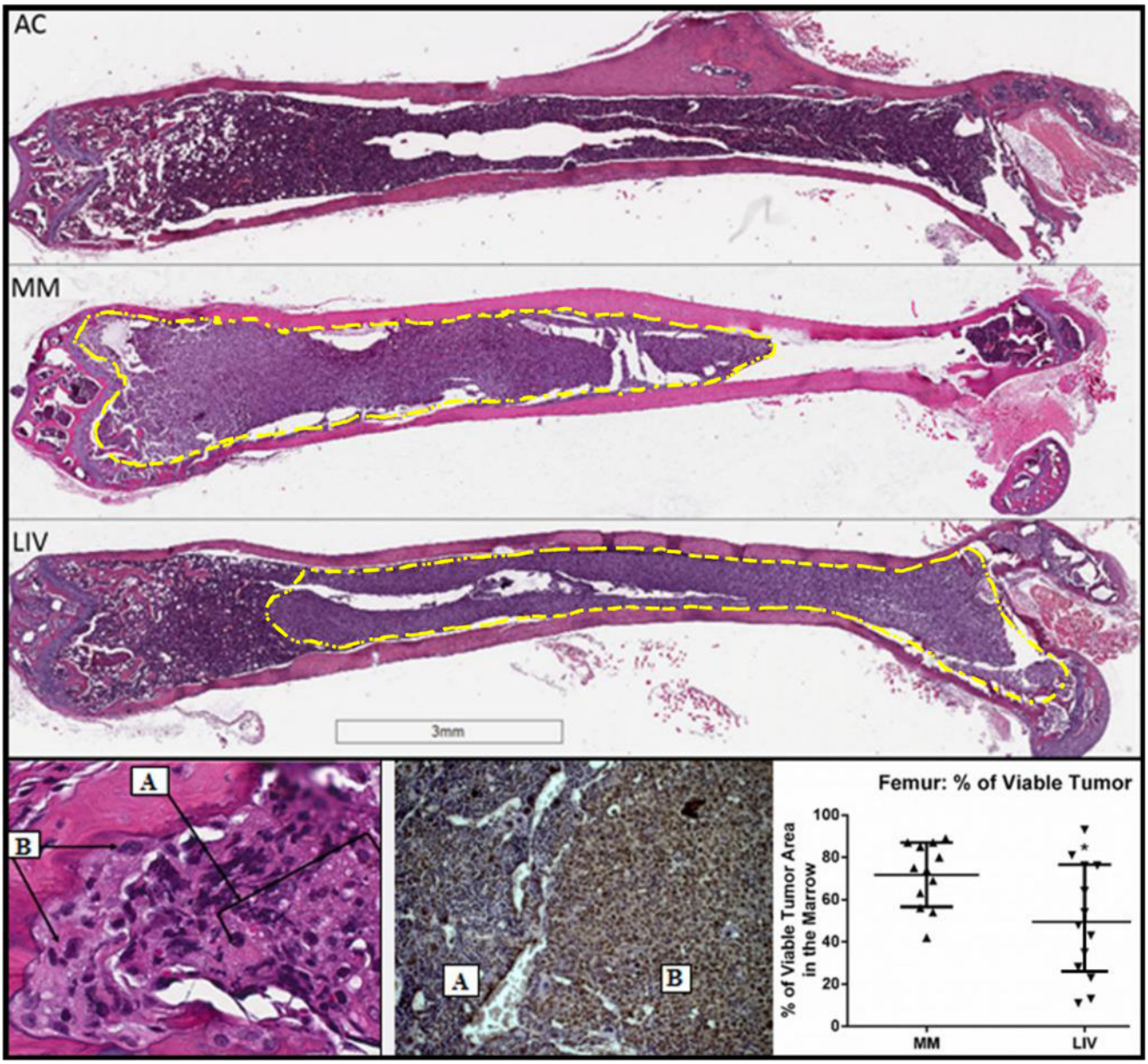

Figure 1.

(Top) Longitudinal 5μm histological sections (0.7×) of H&E-stained femurs across the medullary cavity. AC marrow contained healthy hematopoietic cells throughout the cavity, while cortical bone was unperturbed across the length of the shaft. In MM the confluent tumor burden was evident in the marrow space (yellow-dashed line). A continuous sheet of plasma cells reach to and encroach the growth plate and are found within resorption pits that perforate the cortical shell. Trabecular bone was visibly reduced in MM. Tumor burden was evident in LIV but to a lesser extent than that of MM. Relative to AC, cortical thinning was evident in both MM and LIV, but the resorption was not as pronounced in LIV. **(Bottom Left)** H&E histological section (40×; 5μm) of a cortical resorption pit at the distal femur. Osteolysis was perpetuated by an influx of A.) myeloma cells that have infiltrated the marrow, and B.) osteoclasts, which have subsequently propagated to the bone lining. At the

interface of bone and marrow, the cortical resorption pit demonstrates the relationship between myeloma cells and their capacity to initiate osteoclast-mediated resorption. These sites are surrounded by disorganized, woven bone on the cortex and at the growth plate. **(Bottom Middle)** Antibody staining for $CD138^{+}$ cells demonstrates the delineation of A.) healthy marrow and B.) tumor. **(Bottom Right)** Quantification of viable tumor throughout the femoral BM indicated a 31% reduction in LIV as compared to MM.

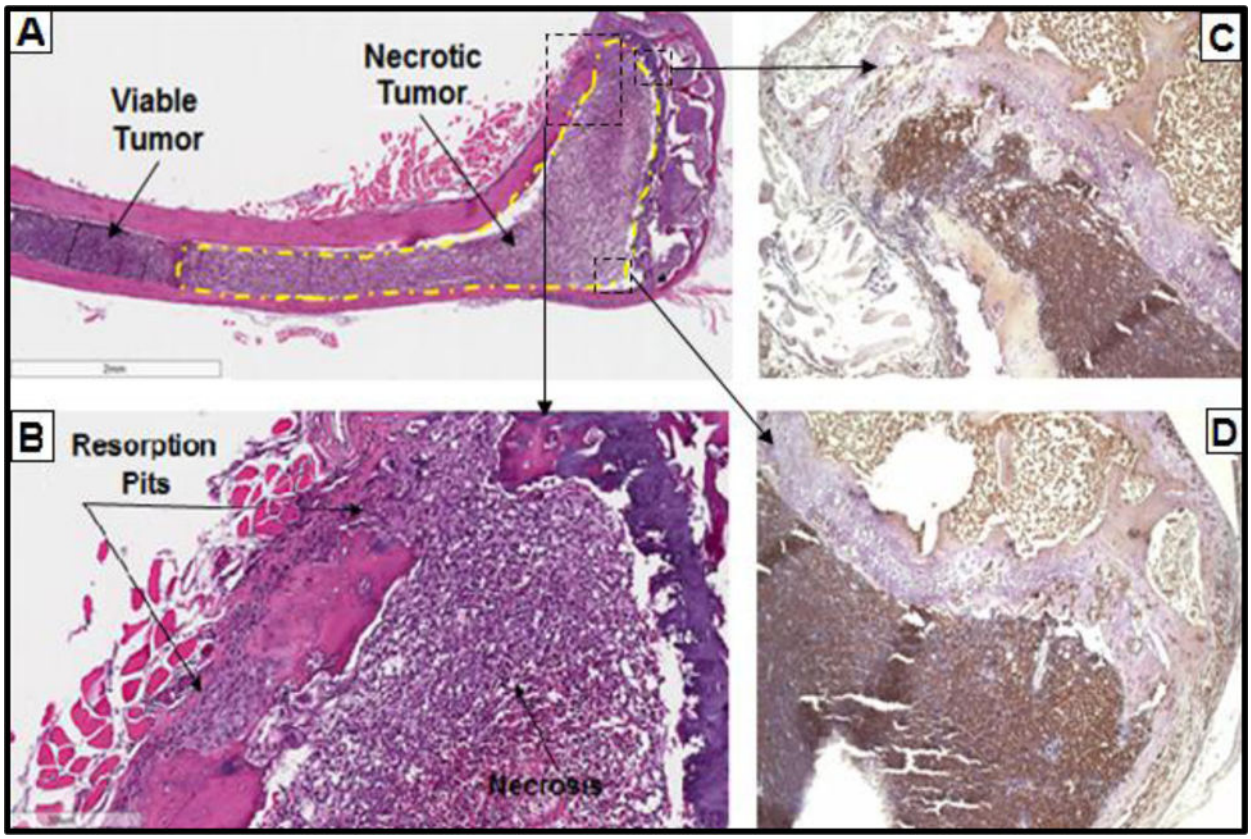

Figure 2.

Histological quantification of viable tumor was performed across the tibial marrow space resulting in 64% occupation of MM marrow, identical to the 63% (NSD) in the marrow of LIV. A.) In contrast to the femur, however, necrotic tumor was observed in 42% of the tibiae of MM group (n=5), as compared to 8% of LIV (n=1), indicating a more advanced stage of disease progression. B.) Note the correlation of osteolytic lesions and resorption to the degree of myeloma cell encroachment in the marrow. Tumor necrosis (Annexin V^+) was evident in the C.) tibial metaphysis and D.) across the growth plate into the epiphysis.

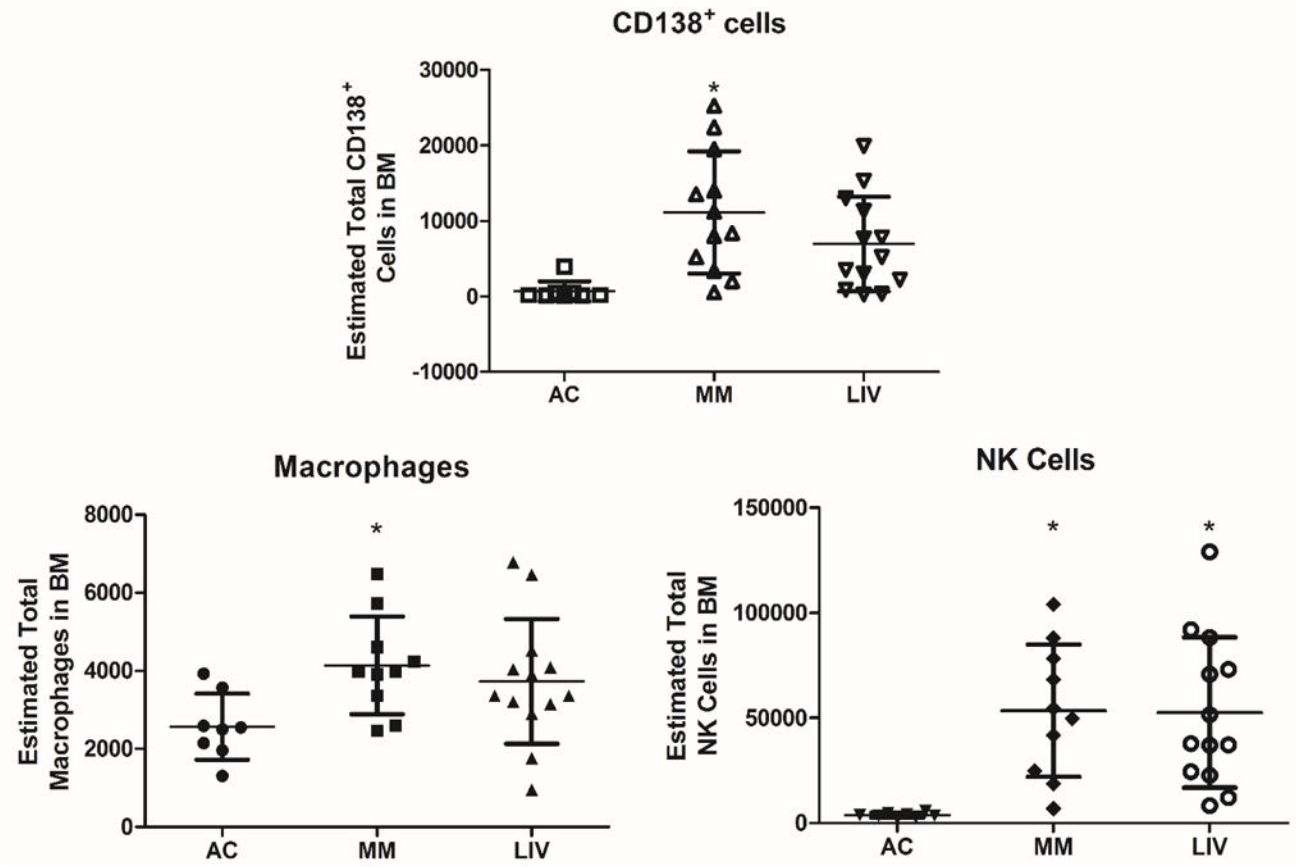

Figure 3.

FACS analysis of hematopoietic components of femoral BM. A.) As compared to AC, FACS of BM from the left femora of LIV showed a 40% decrease of $CD138^+$ cells as compared to MM ($p=0.08$). B.) Total mature macrophages were 61% ($p<0.05$) greater in MM as compared to AC, while there were 26% (NSD) fewer in LIV as compared to MM. C.) Progenitor-NK cells ($NK1.1^+$) in MM and LIV were 1332% ($p<0.003$) and 1310% ($p<0.003$) greater, respectively, than in AC. These data indicate that although the animal is immunocompromised, certain elements of the immune system are still responsive to the disease, here indicated by the level of $CD138^+$ cells in the marrow.

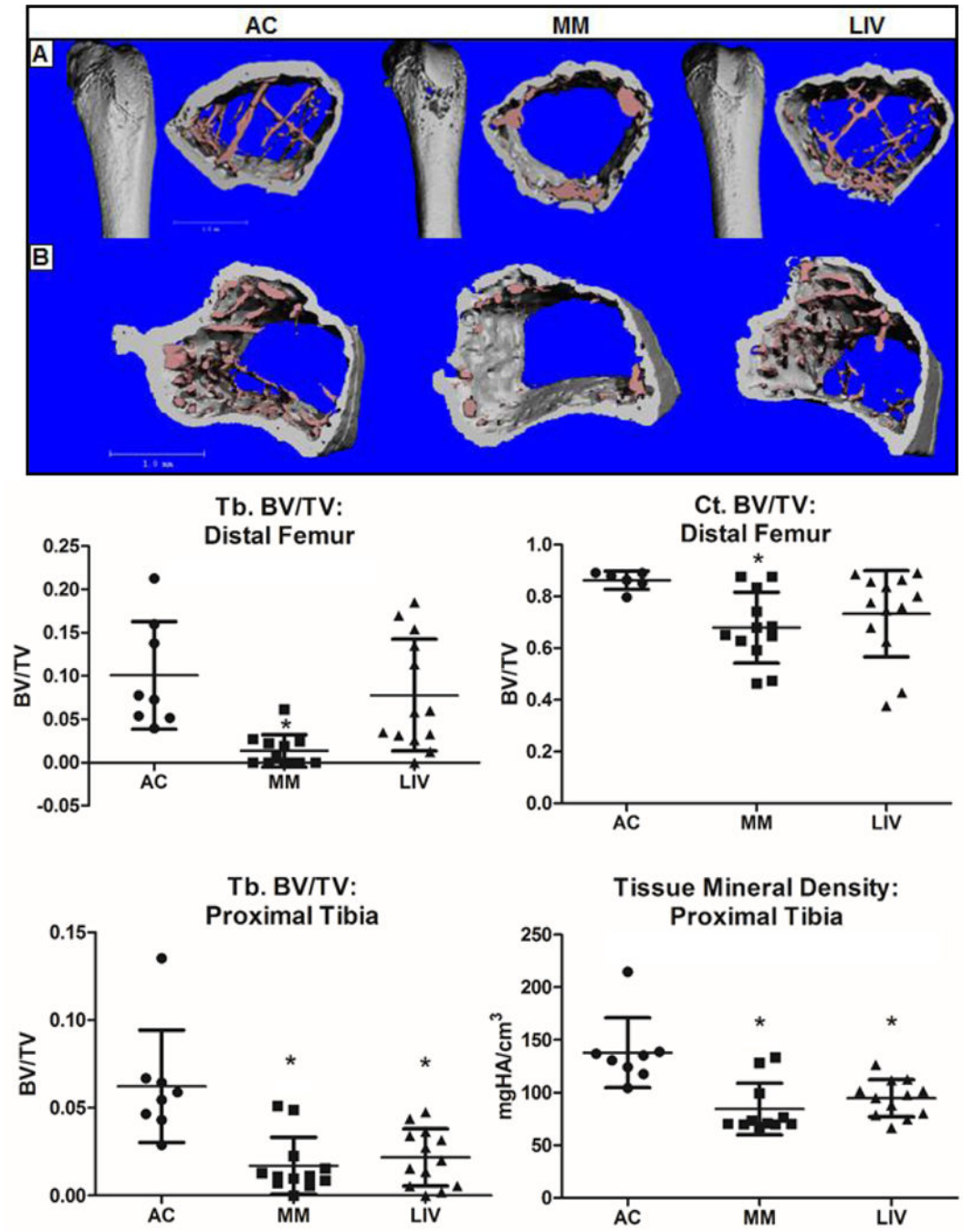

Figure 4.

Micro-CT analysis of segmented bone parameters in the **(Top)** femur and **(Bottom)** tibia were used to measure differences in bone quantity and quality. Quantification of the distal femora revealed an 85% ($p<0.04$) lower trabecular bone volume fraction (Tb.BV/TV) in MM as compared to AC. In contrast, LIV was only 21% lower than AC, reflecting a 75% 'benefit' of mechanical stimulation over MM alone. Cortical BV/TV (Ct.BV/TV) of the femoral metaphysis was 21% ($p<0.03$) lower in MM as compared to AC, while LIV was 15% lower, reflecting a 30% protective benefit of LIV. Tibial Tb.BV/TV across the proximal

tibia was 70% ($p<0.001$) lower in MM as compared to AC, while decreasing by only 62% (NSD) in LIV from AC, a mark 27% greater than in the MM comparison. Tissue mineral density had decreased by 39% ($p<0.001$) in MM as compared to AC decreasing by just 27% ($p<0.002$) in the tibiae of LIV mice.

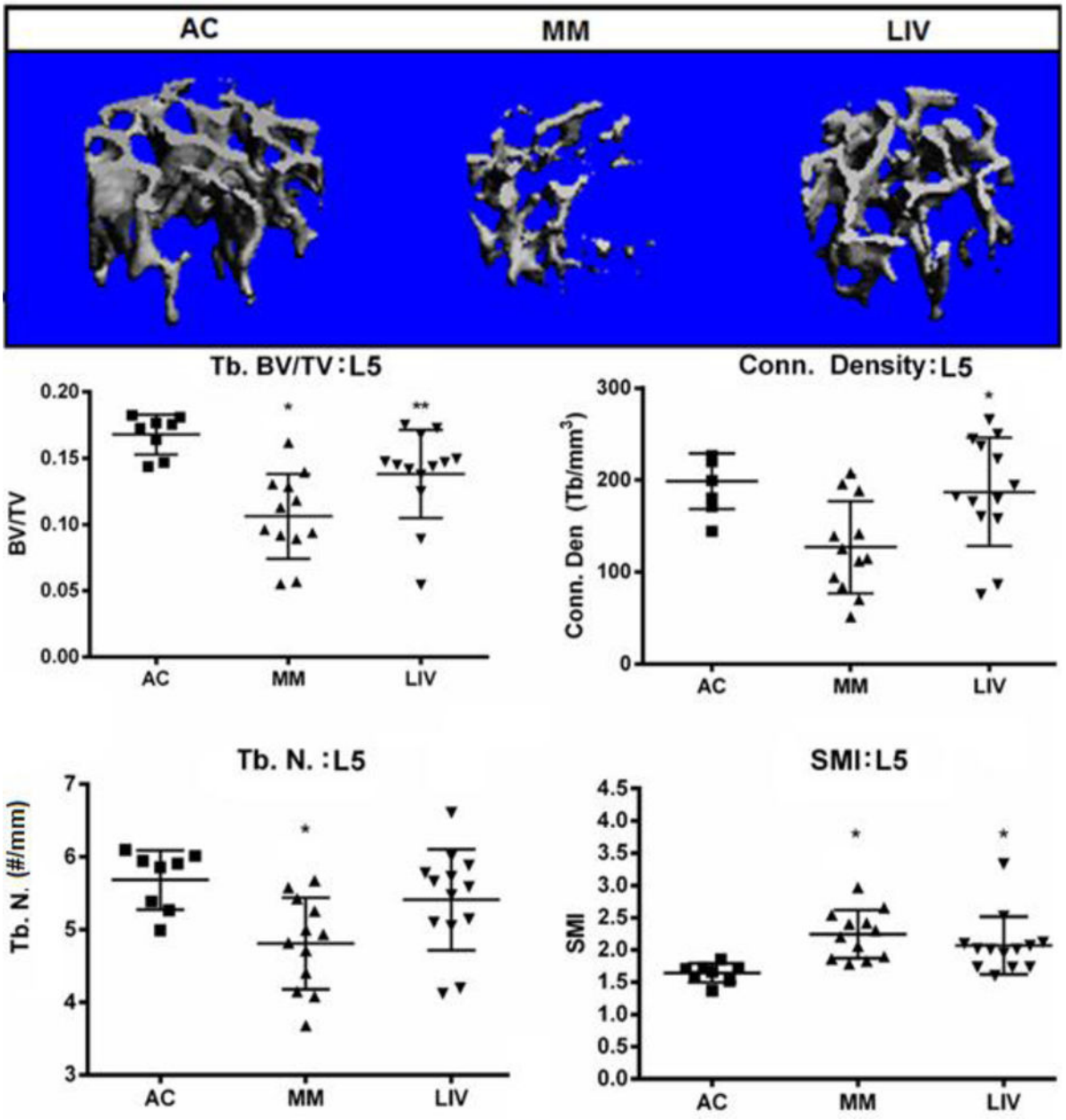

Figure 5.

Representative micro-CT (voxel resolution = 10μm) analysis of the L5 region of the axial skeleton. Trabecular bone was digitally isolated from the cortical shell of the vertebral body in order to quantify bone quantity and quality. BV/TV in MM mice were 35% ($p<0.001$) lower than in AC, LIV mice had 17% (NSD) less bone than AC, a measure that was 27% ($p<0.05$) greater as compared to MM. Trabecular connectivity density in MM mice was 36% ($p<0.05$) lower than in AC, whereas LIV mice were only 6% (NSD) less than in AC, a measure that was 47% ($p<0.05$) greater than those of MM. The number of trabeculae in the L5 of MM had decreased by 16% ($p<0.05$) versus AC while decreasing by just 5% (NSD) in LIV in comparison to AC, a mark that was 13% (NSD) greater than MM. The structure model index (SMI) indicated that trabecular bone was more rod-like in MM and LIV than

AC, as this index was 37% ($p<0.01$) greater in MM than AC, but just 31% ($p<0.05$) greater in LIV than AC.

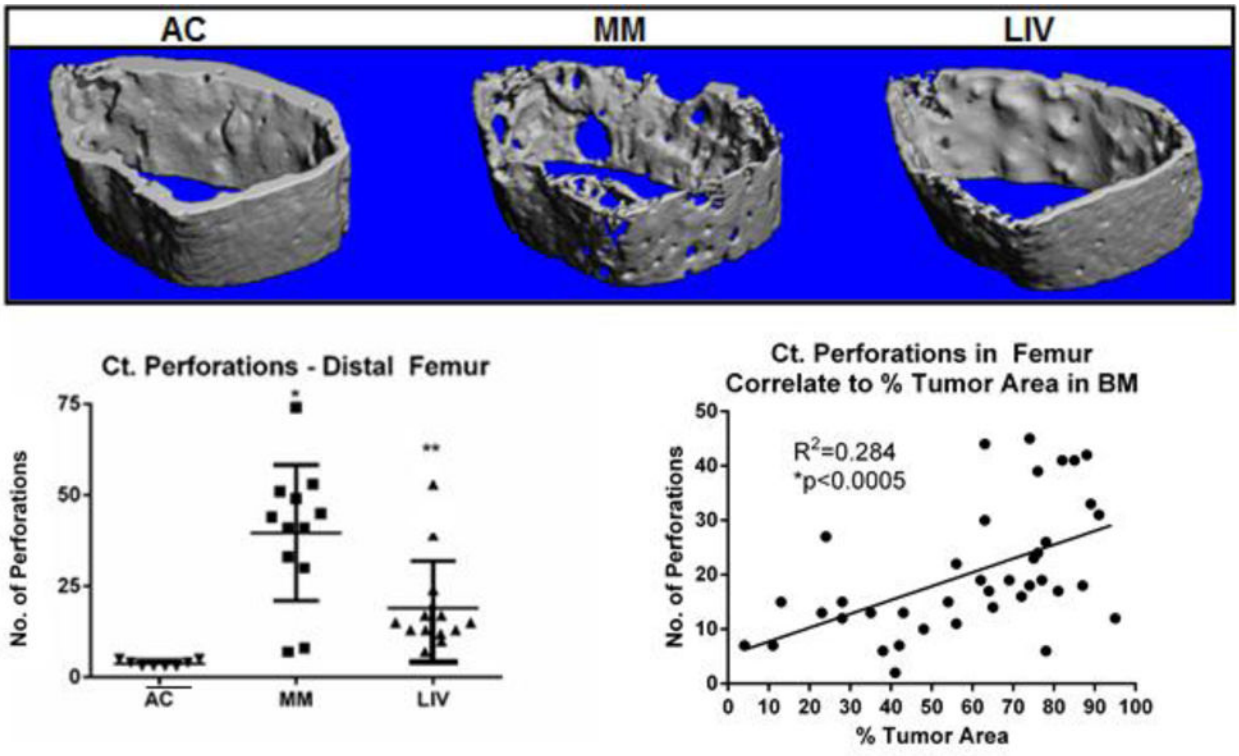

Figure 6.

Representative micro-CT (voxel resolution = 10μm) whole bone and transverse cross-sectional reconstructions of distal metaphyseal region of the femur. **(Top)** AC bones have a uniform, smooth periosteal surface and robust trabecular formation. Severe osteolysis and extensive porosities were observed in MM femora, demonstrating the pathology directly associated with U266β1 engraftment into the medullary canal. LIV bones, while not fully preserved, showed fewer perforations and a greater degree of trabecular conductivity. **(Bottom)** Transcortical perforations in MM were 9× ($p<0.0001$) greater than AC, a deterioration which fell 57% ($p<0.003$) in LIV. A correlation between degree of osteolysis and tumor burden ($R^2=0.284.$; $p<0005$) suggests a strong interaction of the two consequences of the disease.

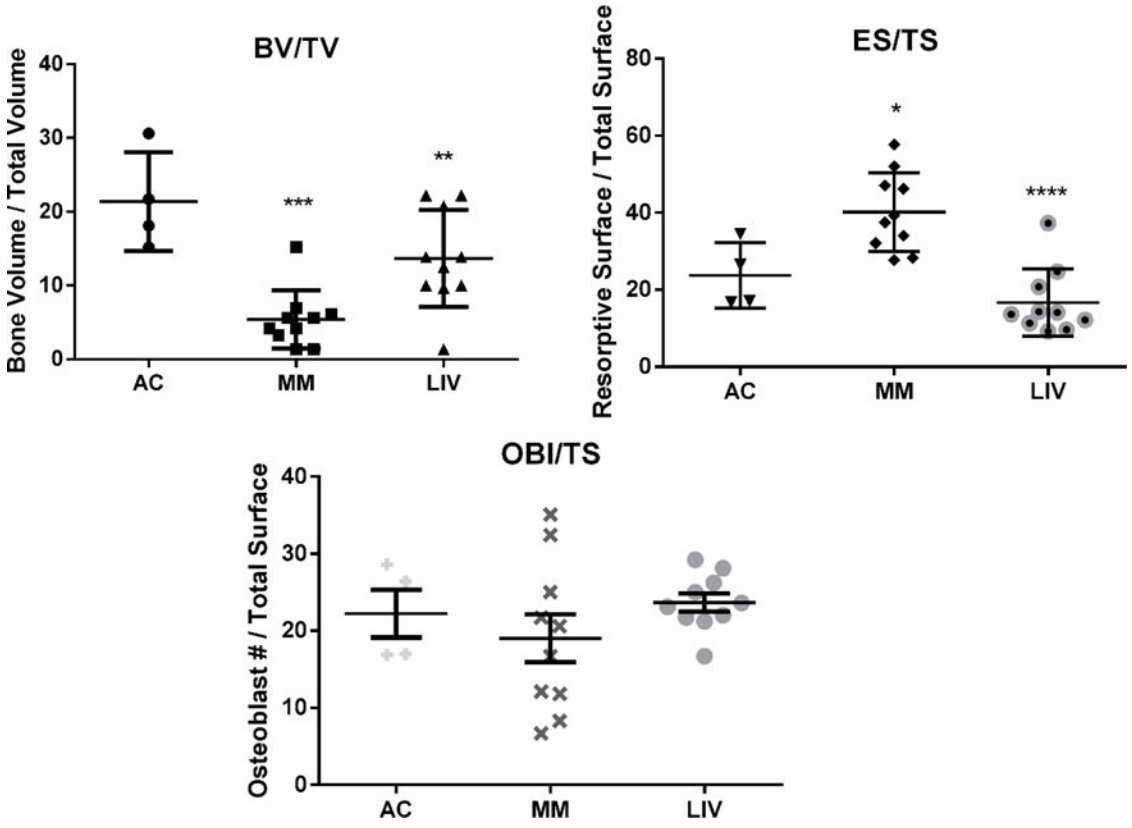

Figure 7.

Static histomorphometry was performed on histological sections of distal femora to discern the degree to which LIV effected resorption or formation. **(Top Left)** BV/TV was significantly reduced ($p<0.0001$) in MM from AC, a mark which improved by 60% ($p<0.001$) in the LIV-treated animals, all of which reflected data quantified via micro-CT analyses. **(Top Right)** As a measure of degree of bone resorption, resorptive surface per total surface was 70% ($p<0.05$) and 29% (NSD) greater in MM and LIV, respectively, as compared to AC. Introduction of LIV appears to have mitigated the degree of resorption by 58% ($p<0.0001$) than in myeloma animals denied LIV treatment. However, as an indication of bone formation, **(Bottom)** osteoblast counts in the same region (OBl/TS) were 14% (NSD) lower in MM as compared to AC mice. LIV appears to encourage a modest 24% (NSD) increase from MM-only mice. Overall, this indicates that a more anti-resorptive mechanism on trabecular surfaces was responsible for mitigating the osteolysis.

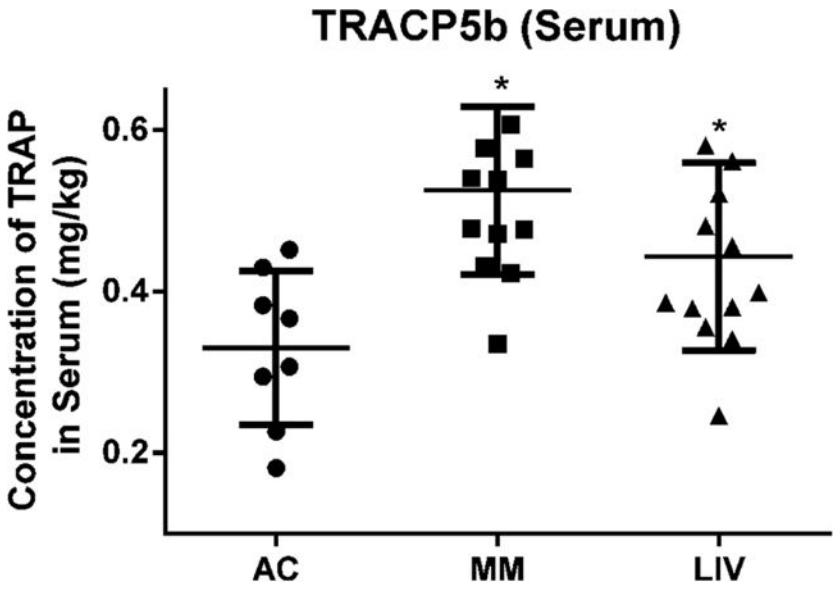

Figure 8.

Immunoassay performed to detect serum-bound tartrate-resistant acid phosphatase (TRACP5b) was isolated from peripheral blood. Significantly greater osteoclast activity was quantified in animals bearing myeloma (MM and LIV), versus those of the AC group. Serum-TRACP5b measured from MM was 61% ($p<0.001$) greater in the MM versus AC. Introduction of LIV reduced serum-quantified osteoclast activity to 33% ($p<0.05$) greater than AC but 45% ($p<0.06$) below detected levels in MM.